Article

Applying High-Resolution UAV-LiDAR and Quantitative Structure Modelling for Estimating Tree Attributes in a Crop-Livestock-Forest System

Ana Paula Dalla Corte , Bruna Nascimento de Vasconcellos , Franciel Eduardo Rex, Carlos Roberto Sanquetta, Midhun Mohan, Carlos Alberto Silva, Carine Klauberg, Danilo Roberti Alves de Almeida , Angelica Maria Almeyda Zambrano , Jonathan William Trautenmüller et al.

land

MDPI

Article

Applying High-Resolution UAV-LiDAR and Quantitative Structure Modelling for Estimating Tree Attributes in a Crop-Livestock-Forest System

Ana Paula Dalla Corte [1,*], Bruna Nascimento de Vasconcellos [2], Franciel Eduardo Rex [1], Carlos Roberto Sanquetta [1], Midhun Mohan [3], Carlos Alberto Silva [4,5], Carine Klauberg [6], Danilo Roberti Alves de Almeida [7], Angelica Maria Almeyda Zambrano [8], Jonathan William Trautenmüller [1], Rodrigo Vieira Leite [9], Cibele Hummel do Amaral [9], Hudson Franklin Pessoa Veras [1], Karla da Silva Rocha [10], Anibal de Moraes [11], Mauro Alessandro Karasinski [1], Matheus Niroh Inoue Sanquetta [1] and Eben North Broadbent [12]

[1] BIOFIX Research Center, Federal University of Parana, Curitiba 80210-170, Brazil; francielrexx@ufpr.br (F.E.R.); sanquetta@ufpr.br (C.R.S.); trautenmuller@ufpr.br (J.W.T.); hudson.veras@ufpr.br (H.F.P.V.); karasinski@ufpr.br (M.A.K.); mateus.samquetta@ufpr.br (M.N.I.S.)
[2] EMBRAPA Florestas, Colombo 83411-000, Brazil; bruna.vasconcellos@cas.ifmt.edu.br
[3] Department of Geography, University of California, Berkeley, CA 94709, USA; mid_mohan@berkeley.edu
[4] School of Forest Resources and Conservation, University of Florida, Gainesville, FL 32611, USA; c.silva@ufl.edu
[5] Department of Geographical Sciences, University of Maryland, College Park, MD 20742, USA
[6] Department of Forest Engineering, Federal University of João Del Rei, Sete Lagoas 35701-970, Brazil; klauberg@ufsj.edu
[7] Department of Forest Sciences, "Luiz de Queiroz" College of Agriculture, University of São Paulo, Piracicaba 13418-900, Brazil; daniloraa@usp.br
[8] Spatial Ecology and Conservation Laboratory, Center for Latin America Studies, University of Florida, Gainesville, FL 32611, USA; aalmeyda@ufl.edu
[9] Department of Forest Engineering, Federal University of Viçosa, Viçosa 36570-900, Brazil; rodrigo.leite@ufv.br (R.V.L.); chamaral@ufv.br (C.H.d.A.)
[10] Geoprocessing Laboratory, Federal University of Acre, Rio Branco 69980-000, Brazil; karla.rocha@ufac.br
[11] Department of Plant Sciences, Federal University of Parana, Curitiba 80210-170, Brazil; anibalm@ufpr.br
[12] Spatial Ecology and Conservation Laboratory, School of Forest Resources and Conservation, University of Florida, Gainesville, FL 32611, USA; eben@ufl.edu
* Correspondence: anacorte@ufpr.br; Tel.: +55-41-3360-4264

Abstract: Individual tree attributes, such as stem volume and biomass, are usually predicted by using traditional field-derived allometric models. However, these models are derived from data collected from small areas and lack a level of detail of tree components (e.g., stem, branches, and leaves). Remote sensing techniques such as the Quantitative Structure Modelling (QSM) applied on high-density LiDAR data emerge as a promising solution for obtaining extensive and detailed tree attribute estimates. We used a high-density LiDAR data on board of a Unmanned Aerial Vehicle (UAV) to evaluate the performance of the QSM approach in estimating field-derived individual tree attributes such as the diameter at breast height (dbh), tree height (ht), and volume (v), as well as the stem (SAGB), branch (BAGB), and total (TAGB) aboveground biomass of eucalyptus trees. QSM was used in two different approaches: (i) using dbh and h derived from QSM and then applied into the field-based equations for estimation of volume and (ii) deriving tree volume directly from QSM. In general, all fitted models using the QSM approach were satisfactory, but with a slight tendency of over-estimation of dbh (9.33%), ht (12.40%), v-QSM1 (26.35%), v-QSM2 (26.66%), TAGB (27.08%), SAGB (25.57%), and BAGB (20.08%). Non-significant differences were noticed when estimating the dbh, tree volume, stem, and aboveground biomass. Despite the overestimation, this study indicates that using the QSM approach to estimate individual tree attributes from UAV-LiDAR is a promising alternative to support the decision-making process regarding forest management activities, especially when considering tree architecture and biomass components.

Keywords: quantitative structure modelling; laser scanning; tree modelling

1. Introduction

Annually, industries and society demand millions of cubic meters of wood [1]. Thus, the decision-making process regarding forest management activities is crucial to meet the demand of these industries [2,3]. Forest industries and farmers demand reliable and accurate information on the availability of different products, such as merchantable volume, to enhance their profitability [4]. However, the uncertainties about these estimates, due to the different methods used, are considerable.

Brazil has more than 10 million ha of forest plantations [5] and around 7 million hectares consist of clonal eucalyptus stands [6]. These plantations are usually focused on pulp and charcoal production. Thus, no distinction in the log's size is imposed (i.e., sawtimber, pulpwood, and charcoal) [2]. However, recent initiatives have ventured into diversifying the clonal eucalyptus production outcomes from Brazilian plantations. Hence, individual-tree-level approaches are needed to provide detailed information regarding tree architecture and multiple product availabilities [7–10].

Under this scenario, both tree volume and aboveground biomass are essential information for planning silvicultural and harvest activities and assessing the environmental and ecological services from forest stands [11–14]. However, their determination may be challenging, depending on the extension and access to these areas and their varying homogeneity levels [15]. Traditionally, tree biomass and volume determination are based on allometric models [16–18]. Despite their efficiency in estimating tree attributes, these models fail to provide detailed information concerning different tree components (e.g., stem, branches, and leaves). In addition, most of these models are limited since they are usually fitted under very specific site conditions, making them inflexible and inaccurate when used for different tree species or genotypes, ages, and sizes [19–21]. Remote sensing technologies, such as light detection and ranging (LiDAR), have emerged to derive three-dimensional (3D) and detailed information from the forest canopy and its structure [22–24].

Several studies have addressed the applicability of LiDAR—ranging from individual tree detection (ITD) to assessing uniformity indices and predicting biomass [25–30]. Terrestrial laser scanning (TLS), with very high density LiDAR data, has become increasingly relevant for providing accurate 3D data about trees [31–33]. Thus, it is now possible to derive several metrics from trees, which are otherwise impractical through direct determination without destructive tree harvesting [34]. Usually, voxelization procedures [35,36] or cylinder assembly algorithms are employed for this purpose [37–40]. However, recent studies suggest using quantitative structure modeling (QSM) [41,42], as this method provides fast and accurate information on different tree components from the TLS point cloud [15,18,43–48].

Despite the benefits of TLS, operational limitations make it difficult to obtain data for large areas. TLS data collection in field surveys is a tiring endeavor, taking 3–6 days to scan 1 hectare in some cases [33]. One disadvantage of UAV LiDAR over TLS is the fact that tree trunks are much easier to delineate from ground-based data (TLS), especially in densely wooded areas. As a result, the use of UAV (Unmanned Aerial Vehicle) technologies has expanded in recent years. A few studies have been developed addressing the use of UAV-LiDAR to generate tree attribute estimates. Biomass studies in the field are expensive and time-intensive. Recent studies, such as [49,50], highlighted the potential of using UAV-LiDAR for assessing individual tree metrics, such as the diameter at breast height, total height, and volume. However, to the best of our knowledge, no studies have been conducted to estimate the aboveground biomass and volume for different tree components using QSM and high-density UAV-LiDAR data. Studies have tested QSM reconstructions of individual trees using UAV-derived point clouds and concluded that it is a promising approach for estimating aboveground biomass [14]. However, in that study, photogrammetry and not LiDAR was used to generate the point cloud. The QSM method uses only the xyz coordinates of the points to construct the geometric and topological properties of the trees stored in the models. Therefore, with LiDAR having greater penetration into the forest interior, generating denser (XYZ) coordinates than photogrammetry, it is expected

that QSM combined with it will help better explain the biomass. Most related studies using QSM were based on TLS 3D point clouds. In this study, we aimed to evaluate the performance of high-density UAV-lidar and the QSM approach for estimating individual tree attributes, such as diameter at breast height (dbh), total height (ht), and volume (v), as well as the stem (SAGB), branch (BAGB), and total (TAGB) aboveground biomass in eucalyptus stands established in a crop–livestock–forest system. Our hypothesis is that the QSM method can estimate biomass, as well as in the field on high-density UAV-LiDAR data.

2. Materials and Methods

2.1. Study Area

This study used data from a 17 ha eucalyptus plantation (Eucalyptus benthamii Maiden et Cambage) established in a crop–livestock–forest system—iCLF (Figure 1)—at age 6 years. Crop–livestock–forest integration (ILPF) is a production strategy that integrates different production systems, agricultural, livestock, and forestry, within the same area. It can be used in intercropping, in succession, or in rotation, so that there is mutual benefit for all activities. The plantation is located in the municipality of Pinhais, Paraná State, southern Brazil (25°22′38″ S, 49°09′05″ W). According to the Brazilian System of Soil Classification, study area soils are classified as Haplic Cambisol [51]. This soil order corresponds to Inceptisol in soil taxonomy [52]. The study area is characterised by a humid subtropical climate with oceanic climate—Cfb (without a dry season and temperate summer)—with an annual rainfall of 1550 mm [53]. Additionally, the average elevation is ca. 920 m above sea level. The initial tree spacing was 2×14 m, totaling 357 trees per hectare. The large spacing is a characteristic of the iCLF.
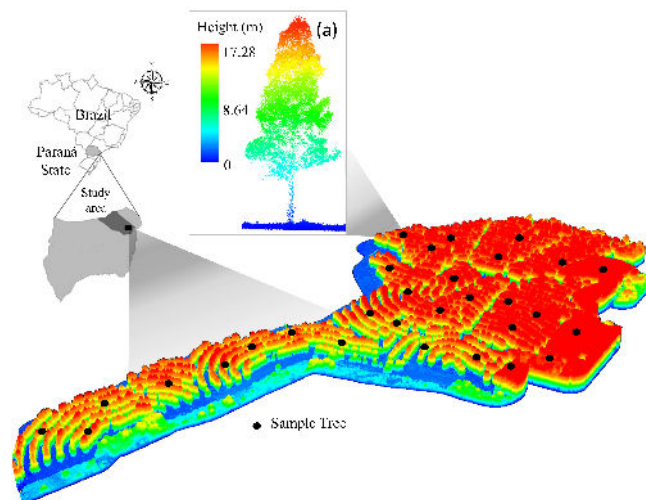
Figure 1. Location of the study area in Southern Brazil with the UAV-LiDAR 3D point Cloud and the 30 selected sample trees (black points) for QSM application: (**a**) Detail of the normalized point cloud of a selected tree.

2.2. Field Data

A total of 30 trees were randomly selected for field sampling. These trees were randomly selected in order to comprise the stand amplitude regarding dbh (diameter at 1.3 m above the ground) and total tree height (ht) structure. These trees were felled, bucked, and scaled. On each tree, measurements of the stem were taken at various heights along the tree trunk. For every section, volume was obtained from the Smalian's formula (which involves the average cross-sectional area of the large and small ends times the log length) (Equation (1)):

$$v = \frac{g_1 + g_2}{2} * l \tag{1}$$

where: v = log volume (in m^3); g_1 = cross-sectional area of the large end (in m^2); g_1= cross-sectional area of the small end (in m^2); l = log length (in m).

Total aboveground biomass (TAGB) was determined by weighing tree components separately (stem—SAGB and branches—BAGB) using a 100 g precision dynamometer and summing up the total AGB per each tree. Samples of 1 kg were collected from each tree and biomass component for dry matter determination and were oven-dried at 70 °C until they reached a constant weight

2.3. UAV-LiDAR Data Collection

The UAV-LiDAR data were obtained in September 2019 with the GatorEye system. The GatorEye comprises DJI Matrice 600 Pro hexacopter capable of 16–22 min flight times for small areas (<20–30 acres·flight^{-1} and 10 battery packs) and with a 5 km telemetry/control range. The GatorEye system has a Phoenix Scout + core with a tactical-grade Novatel STIM 300 IMU and differential GNSS system. After the post-processing of a smooth trajectory in Novatel Inertial Explorer, the LiDAR point's absolute precision was within about 5 cm repeatable [54], with greater relative accuracy between points collected from the same flight line. The GatorEye system includes a sensor called Velodyne VLP-32c LiDAR puck sensor [55]. The flying height was 55 m above the ground at a speed of 8 ms^{-1} and at an approximate horizontal distance between the adjacent flight lines of 15 m, producing a very high-density LiDAR point cloud (1400 points per meter squared). The UAV flight lines provide for redundant coverage in the area (overlap of 90%). Additionally, returns were limited to those having a range of less than 100 m and a field of view of 120 m.

Lidar Data Processing

The first steps of LiDAR data processing used Lastools functions [56]. High-density 3D points were merged using lasmerge (LasTools) and clipped within the study area using the lasclip tool (LasTools). Subsequently, lasnoise (LasTools) was applied to identify and remove spurious returns. The next steps was in R environment [57], where the ground returns were classified using lasground new; then; the digital terrain model—DTM—was designed with las2dem (0.5 m resolution). DTM was used to designed the normalized lidar point clouds (lasheight) and the canopy height model—CHM (0.5 m resolution).

The next step used the CHM and the normalized LiDAR point clouds as inputs for individual tree detection. The dalponte2016's ITD algorithm [58,59] was used to delineate and segment single tree crowns within the 3D point cloud (Figure 2). The Dalponte2016 algorithm finds the maximum locations within a CHM image, representing the treetop, and then uses a decision algorithm to outline trees' crowns around the maximum locations. For this, an LMF was applied over the CHM with a window of 3 m × 3 m, trying to find the highest point. According to authors in [59], the LMF technique is used with images with the assumption that the reflectance of a treetop is typically higher at its apex.

Similarly, the LMF assumes that the higher laser elevation point for the same tree crown consists of its apex. When the LMF is used in a point cloud to deal with this, it assumes that the highest laser value between the laser strokes of the same tree crown is the apex. When several pixels present the same value in the CHM, the whole-mass center of these pixels is considered the tree apex. Thus, these maximum locations express the top positions of the identified trees. Then, the associated CHM value is extracted to define the top heights of the trees. In [58], the authors highlight this approach by describing the following steps: (i) a low-pass filter applied to rasterized CHM to smooth the surface and reduce the number of local maxima; (ii) define the local maxima using a moving window (3 × 3 m in this case); a CHM pixel is labeled as local maxima if its value is higher than all other values in the window, as long as it is higher than some minimum height above ground; (iii) each local maximum is labeled as an "initial region" around which a treetop can grow; the heights of the four neighboring pixels are taken from the CHM, and these pixels are added to the region if their vertical distance of the maximum location is less than some user-defined percentage of the local maximum height, and less than some user-defined maximums difference. This procedure is repeated for all cell neighbors now

included in the region, and so on, until there are no more pixels added to the region; (iv) of each region that had been identified, the first return cloud points are extracted (having first removed low elevation points); and (v) a 2D convex hull is applied to these points, and the resulting polygons become the final individual tree crowns. All steps of the dalponte2016 algorithm were employed using the LidR package in R [57–59].
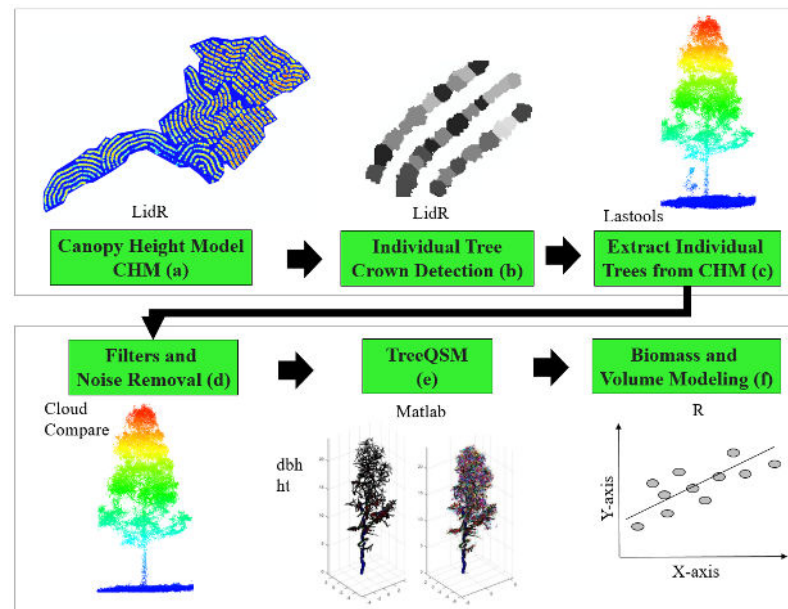

Figure 2. Diagram of UAV-LiDAR point cloud processing: (**a**) pre-processing; (**b**) ".las" normalized and Canopy Height Model—CHM; (**c**) Individual Tree Crown Detection; (**d**) Extract Individual Trees from CHM; (**e**) Filters and Noise Removal; (**f**) Result of TreeQSM.

With trees identified, we performed a random sampling to select 30 trees for further analysis, and the lasclip tool was applied to cut the normalized LiDAR point clouds to the trees. Quantitative structure modeling (QSM) was used to assess tree architecture [15]. For this purpose, point clouds containing one tree at the time were delimited. QSM is a semi-automatic method that builds a tree model from laser scanner point clouds and consists of a hierarchical collection of cylinders of calculable volume. The QSM algorithm implemented in the TreeQSM function in MATLAB assumes that most points consist of stems and branches, and the QSM uses these points to build the cylinders. When removing phantom points (e.g., noise points from leaves) was necessary, we applied the filtering function (Equation (2)) in MATLAB R2020b.This filtering formula and the other procedures of the TreeQSM algorithm (version 2.4.0) are described in detail in the manual [15,46]:

$$filtering(P_0, r_1, n_1, d_2, r_2, n_2, Scaling, AllPoints) \qquad (2)$$

where: P_0 = unfiltered point cloud; r_1 = radius of the balls used in the first filtering (defines the volume); n_1 = minimum number of points in the accepted balls of the first filtering; d_2 = minimum distance between the centers of the balls in the second filtering; r_2 = radius of the balls used in the second filtering; n_2 = minimum number of balls in the components passing the second filtering; Scaling (optional input) = if true, the first filtering threshold n_1 is scaled along with the height with average point density (default value false); *AllPoints* (optional input) = if true, performs the first filtering process for every point (default value false). Point cloud filtering aims to eliminate points based on the distance threshold between neighboring points, intensity value, or density of points along the surface of the stem.

Then, the variables of the model were established: PatchDiam-parameter (pd)—the average size of the cover sets is controlled by the minimum patch diameter (0.2) and the maximum (0.8); the branching order of the QSM has been set to add a level to each branch node. QSM partitioned the point cloud into small connected surface patches and used them

to reconstruct each tree segment. Then, cylinders were created and fitted into the segments, creating a 3-dimensional reconstitution of the tree structure [37,43,60,61]. From the 3-dimensional reconstitution of the tree were extracted the metrics of dbh, total tree height, volume, and branch structure. Two different approaches were evaluated when predicting tree volume (QSM1 and QSM2). The QSM1 approach was built using dbh and ht derived from TreeQSM and then applied into the field-based equations for estimation volume. On the other hand, QSM2 consisted of deriving tree volume directly from QSM cylinders.

2.4. Data Analysis

To estimate tree volume and biomass using field-based data, we fitted linear regression models [62] using Equation (3). In this step, the lm() function within the software R was used:

$$y = \beta_0 + \beta_1 (dbh^2 ht) \tag{3}$$

where: y = estimated tree attribute (tree volume (in m^3), aboveground biomass, or component biomass (in kg)); dbh = diameter 1.3 m above the ground (in cm); ht = total tree height (in m).

The dbh and ht derived from QSM were used to estimate tree volume and biomass in the compartments (TAGB, SABG, and BAGB). The performance of the fitted equations when predicting tree attributes using QSM-derived metrics were evaluated by assessing the relative root mean square error (rRMSE%), Bias (%), and the coefficient of determination (R^2). Additionally, the paired Mann–Whitney (MW) test examined significant differences between QSM-derived and field-based estimates. MW examines the differences between medians and shape and spread distribution. The *p*-value is contrasted against the significance level to determine whether the median's difference in median values. The null hypothesis (H_0) is rejected when the *p*-value $\leq \alpha$ ($\alpha = 0.05$), indicating significant differences between observed and estimated values. Otherwise, H_0 is accepted (when *p*-value $> \alpha$), suggesting non-significant differences.

Graphical analyses with a scatter plot with the line of equality (1:1 lines) were used to assess the behavior of the estimates, contrasting predicted and observed values from field-based data, as well as QSM1 and QSM2. The scatter plot with the equality line (1:1 lines) highlights how close H_0: $\alpha = 0$ (intercept) and β approaches 1 (slope).

3. Results

3.1. Field-Based Metrics and Allometric Equations

All models displayed significant fitted coefficients (*p*-values) when predicting tree volume, TAGB, SAGB, and BAGB. Figure 3 displays the fitted model's behavior, indicating the traditional modeling approach's satisfactory performance based on field data (Table 1). In general, all fitted equations presented satisfactory goodness-of-fit statistics, with R² ranging from 0.96 to 0.98, and the rRMSE ranging from 8.76 to 40.72%. The correlation (r) between predicted and observed values ranged from 0.86 to 0.99 (Figure 3).

Table 1. Fitted coefficients and their standard errors when predicting tree volume (v), total aboveground biomass (TAGB), stem biomass (SAGB), and branch biomass (BAGB).

| Variable | Mean | SD | Min | Max | Fitted Coefficients (±SE) | | R^2 | RMSE | rRMSE (%) |
					α	β			
Volume	0.73	0.39	0.08	1.50	5.7×10^{-2} (2.2×10^{-2})	3.1×10^{-5} (8.7×10^{-7})	0.97	0.058	8.76
TAGB	406.32	227.35	50.74	867.63	23.52 (18.1)	0.176 (7.22×10^{-4})	0.98	52.8	13.02
SAGB	318.22	170.76	34.80	688.31	33.9 (16.06)	0.0131 (6.4×10^{-4})	0.96	47.02	14.77
BAGB	63.65	50.69	3.25	192.94	−12.11 (8.85)	0.0035 (3.5×10^{-4})	0.96	25.91	40.72

Note: SD—standard deviation; Min—minimum value; Max—maximum value; R^2—coefficient of determination; RMSE—root mean squared error; rRMSE—relative root mean squared error (in %); all other variables were previously defined.
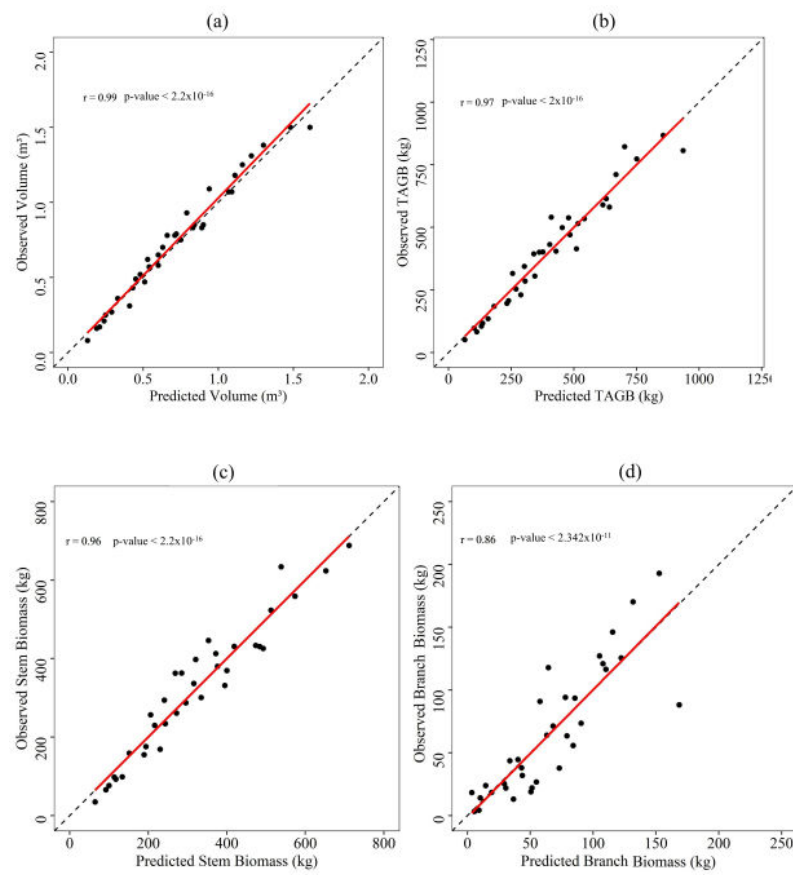
Figure 3. Relationship between observed and predicted tree volume (v) (**a**); total aboveground biomass (TAGB) (**b**); stem biomass (SAGB) (**c**); and branch biomass (BAGB) (**d**).

3.2. QSM-Derived Tree Metrics

3.2.1. Tree dbh and Total Height

The diameter at 1.3 m above the ground (dbh) and tree height (ht) for the 30 individual trees were estimated through the QSM approach. In general, both the dbh (Bias = 1.22 cm; and rRMSE = 9.33%) and ht (Bias = 1.85 m; and rRMSE = 12.40%) estimates showed satisfactory performance (i.e., rRMSE $\leq$ 15%). The Pearson correlation between the field-based and QSM-derived values were r = 0.6 5 (dbh) and r = 0.85 (ht), respectively. Both scatter plots with the line of equality (1:1 lines) presented similar patterns, in which we noticed a slight bias of overestimation for larger values (Figure 4). The Mann–Whitney test indicated a non-significant difference between QSM-derived and field-based data regarding dbh values (p-value = 0.251). Meanwhile, ht estimates presented higher bias (9.33%) when compared to dbh. The QSM approach tends to overestimate tree height, regardless of tree size. Other methods of height estimation could have been tested, for example, rescue directly from the CHM. Since the paper wished to find out how the QSM algorithm would perform, no other methods were tested. We noticed that more than 80% of tree heights were overestimated (Figure 4b), resulting in significant differences by the Mann–Whitney test (p-value $\leq$ 0.05) (Table 2). Although the correlations of LiDAR height estimation and field data are higher in the literature, in this work, the estimation was performed by the QSM algorithm.
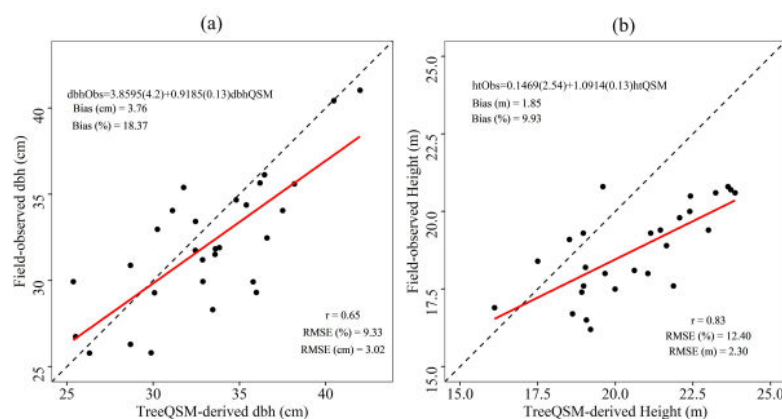
Figure 4. Relationship between QSM-derived and field-based diameter at breast height (dbh) (**a**) and total tree height (ht) (**b**), where observed data are measured in the field.

Table 2. Mann–Whitney test (95% probability) for QSM-derived tree dbh, total height (ht), volume (v), and biomass (TAGB, SAGB, and BAGB).

Metric	Mann	*p*-Value
dbh (observed and *QSM*-derived)	372	0.251
ht (observed and *QSM*-derived)	258	<0.001
TAGB (observed and *QSM*-derived)	316	0.051
SAGB (observed and *QSM*-derived)	316	0.051
BAGB (observed and *QSM*-derived)	316	0.048
v (observed and *QSM1*-derived)	316	0.051
v (observed and *QSM2*-derived)	335	0.092

3.2.2. Stem Volume

Tree volume estimates through QSM1 and QSM2 resulted in similar patterns, in which the rRMSE ranged from 26.35% (QSM1) to 26.66% (QSM2). In both cases, we noticed a slight tendency of overestimation, especially for larger trees (Figure 5). The QSM1 approach consisted of deriving both dbh and total tree height (ht) and applying them into the fitted equations from Section 3.1, while the QSM2 derived the tree volume directly from point cloud cylinders. In general, QSM1 presented smaller errors for larger trees when compared to QSM2. Despite higher relationship between QSM1-derived and field-based values (r = 0.88), most values were placed under the 1:1 line, resulting in larger bias (Bias = 0.12 m^3, rRMSE% = 17.87%). The Mann–Whitney test, however, indicated non-significant differences between individual tree volume derived from TreeQSM, regardless of QSM approach (i.e., QSM1 *p*-value = 0.051, and QSM2 *p*-value = 0.092). Despite similar rRMSE% values, the lower bias and higher *p*-value suggested the superiority of QSM2.

To illustrate the overall performance of the QSM in predicting tree attributes, we displayed two point clouds representing the tree architecture (Figure 6). In the first case, we noticed a higher density of points, in which the volume estimate reached a small error (10.9%) through QSM2 (Figure 6a). In contrast, a cloud of points with lower density made it challenging to examine tree architecture (Figure 6b). As a result, the error in estimating tree volume was higher (25.1%) in this case.

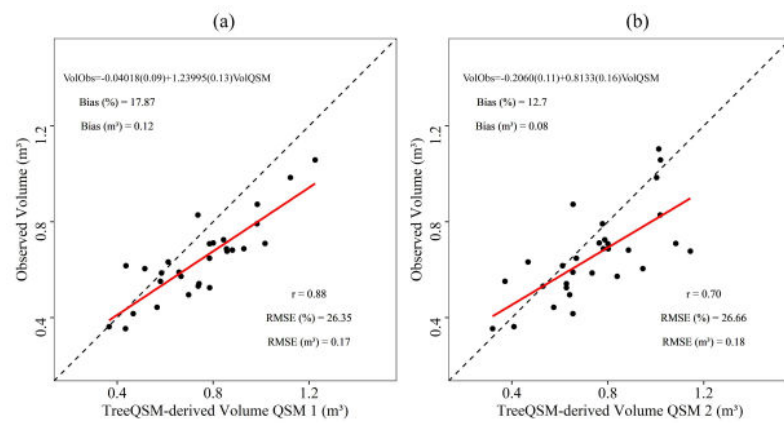**Figure 5.** Relationship between individual field-based and QSM-derived tree volume from QSM1 (**a**) and QSM2 (**b**).
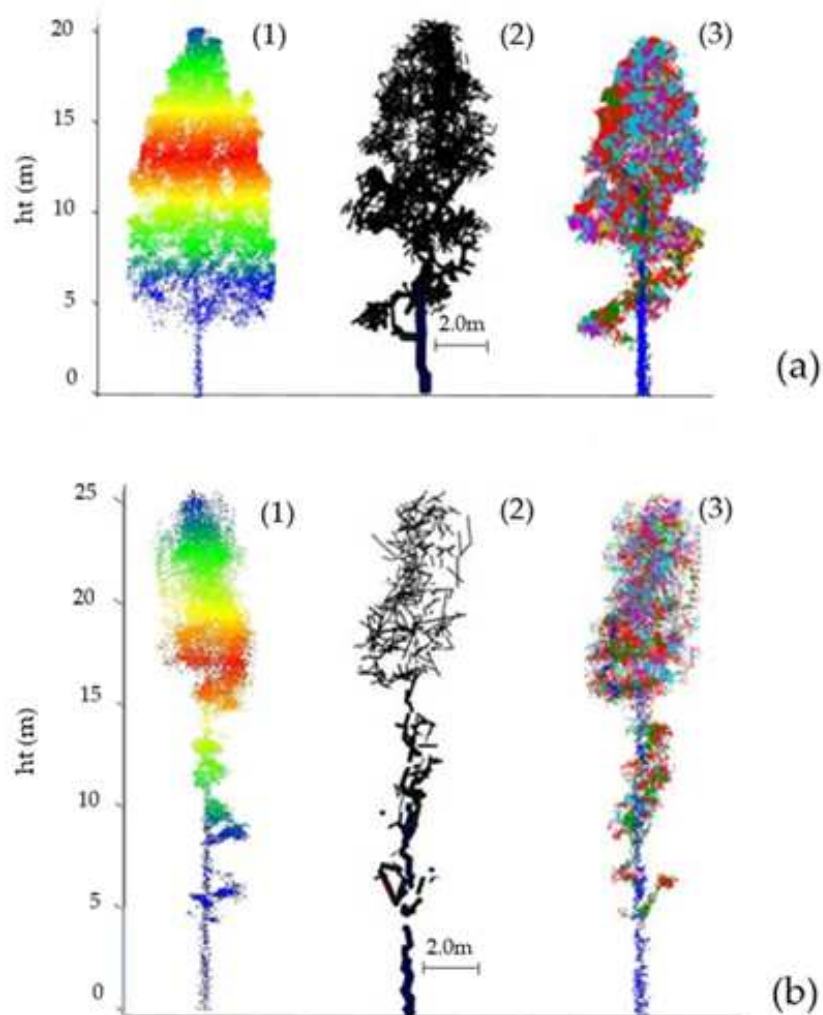

Figure 6. Contrasting density of points in the representation of tree architecture: (**a**) Example of a tree with satisfactory point density; (**b**) Example of a tree with lower point density. (1) Tree point cloud; (2) Structure model of the tree; (3) Automatically reconstructed tree model.

3.2.3. Tree Biomass

Figure 7 displays the overall pattern of the QSM approach when predicting tree biomass (TAGB, SAGB, and BAGB). In general, all biomass estimates presented a similar behavior, in which we noticed a tendency of overestimation for larger trees. This pattern displaced the scatter plot 1:1 line of equality and resulted in positive biases. Despite this, high correlation coefficients were observed (r ranging from 0.87 to 0.88). The rRMSE ranged from 20.08% (BAGB) to 27.08% (TAGB), and non-significant differences were highlighted by the Mann–Whitney test (TAGB *p*-value = 0.051, SAGB *p*-value = 0.051, and BAGB *p*-value = 0.048).

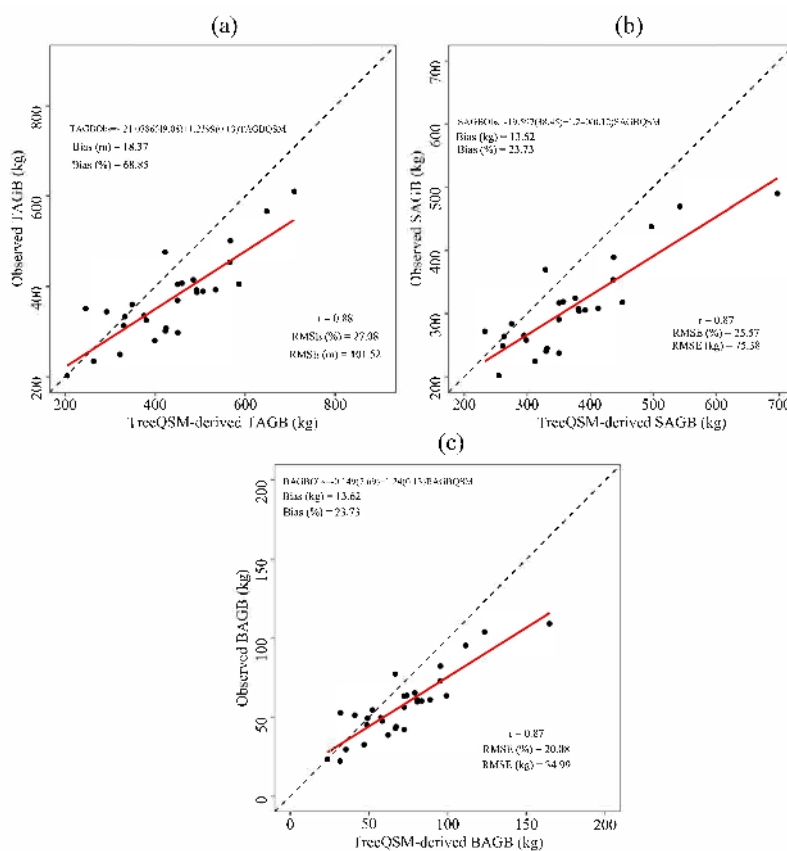The QSM approach also presented an overestimation tendency when deriving both the dbh and ht (see Section 3.2.1).

Figure 7. Relationship between field-observed and QSM-derived biomass estimates: (**a**) Individual tree TAGB (kg); (**b**) Individual tree SAGB (kg); (**c**) Individual tree BAGB (kg).

4. Discussion

The increasing demand for timber implies the necessity of fast and reliable methods capable of providing individual-tree and stand-level attributes [63]. Data collection based on traditional methods (field-based) is costly and laborious [64], especially as it requires harvesting trees to fit allometric equations and measure trees in plots for inferences. Thus, remote sensing approaches, such as LiDAR, have emerged, as they increase data collection and allow assessment at different levels of detail [65,66]. The aerial LiDAR approach is commonly used for large-scale surveys, e.g., [67], from which it is possible to derive several pieces of information regarding forest canopy, such as the Canopy Height Profile—CHP [68]. However, the low point density causes many limitations in ALS applications for the level of individual trees [49,65–68].

In contrast, the TLS system is frequently used for assessing individual trees' structure and architecture [69,70]. The TLS approach provides a higher density of points, which

allows for a 3D characterization. However, TLS has operational limitations regarding data collection, as it requires scanning from different positions to ensure accurate characterization [71–74]. Hence, UAV-LiDAR technology has expanded in recent years, as it combines high density and fast data collection [75]. The use of UAV-LiDAR for assessing individual tree structure is still a novelty [14], especially using the QSM approach. The QSM allows the assessment of different tree components, such as the stem and branch structure.

For the first time, in this study, we examined the performance of QSM using UAV-LiDAR data in predicting individual attributes of eucalyptus trees in a crop–livestock–forest system. Eucalyptus plantations in crop–livestock–forest systems are established in different conditions than most eucalyptus plantations in Brazil [76]. In our case, stand density is quite lower, promoting a more complex branch structure for canopy closure. Thus, trees with larger light interception areas and, consequently, greater solar radiation use efficiency tend to have a more complex crown structure. This fact may justify the challenging assessment of some individual attributes (Figures 4, 5 and 7).

Tree height measurement is difficult in some cases [77]. In addition to the operator's experience, environmental and stand conditions can lead to gross errors in field surveys. In addition, several studies have reported the challenging assessment of crown-level metrics even in field-based surveys, resulting in higher errors when predicting crown or branch biomass than those found for tree volume or stem biomass [78]. Despite this, the QSM approach performed well when deriving most of the individual tree attributes. Errors ranged from 9.33 to 12.40% for QSM-derived tree dbh and total tree height (Figure 4). A slight tendency of overestimation and significant differences in total tree height estimates were noticed. We believe that employing both QSM-derived dbh and total tree height as input in allometric equations may explain the same pattern in volume and biomass estimates (Figures 5 and 7). In a similar study [14], the authors evaluated the performance of the QSM approach using UAV-LiDAR data. These authors noticed significant differences when deriving tree dbh in addition to errors larger than 49 percent when estimating the aboveground biomass.

There is a lack of studies addressing the biomass estimation for different tree components. The QSM approach still has limitations in defining and segmenting cylinders which might lead to the overestimation of tree attributes. In addition, gaps along the tree profile can hinder an accurate assessment of tree structure. We noticed that some trees displayed a lower density of points, resulting in higher errors (Figure 6). Trees located close to stand edges usually tend to present a lower density of points due to the flight path. In this sense, proper flight planning is crucial for ensuring a sufficient density of points for all trees within the stand. Despite the lower density of points in comparison with point clouds collected using TLS, the UAV technology allows the UAV-LiDAR sensor's repeated scanning without exhaustive data collection. Other factors may influence the QSM's accuracy, such as the stand age (influencing stem profile and canopy closure), land slope, and scanning angle [37,46,79,80].

These results suggest that accurate estimates of individual tree attributes (dbh and ht) are crucial for reaching reliable biomass estimates.

To our knowledge, this study is the first initiative that addresses the use of high-density UAV-LiDAR and (integrated) QSM method to assess the biomass of different tree components. Reliable assessments of branch structure are essential to assist the decision-making process regarding silvicultural treatments. Eucalyptus plantations established in crop–livestock–forest systems are usually conducted in longer rotations than those focused on pulp production. Hence, it is possible to increase forest profitability by scheduling pruning and thinning interventions. The use of remote sensing tools such as UAV-LiDAR technology can reduce monitoring costs and data collection time.

5. Conclusions

This study demonstrated the innovative potential of high-density UAV-LiDAR and the QSM approach in deriving individual attributes of eucalyptus trees established in an iCLF system. Despite the overestimation bias, the QSM-derived volume and aboveground

biomass showed non-significant differences compared to field-based data, suggesting the potential of UAV-LiDAR for the non-destructive assessment of tree biomass. Because of this fact, the QSM approach can be used in biomass studies now with high-density UAV-LiDAR data. This fact enables greater scope and area for these studies. The combination of high-density UAV-LiDAR and the QSM approach can help forest monitoring and reduce the cost and time of large-scale biomass estimation and volume forecasting. Future studies should be conducted to address the limitations and influencing factors in QSM-derived metrics accuracy. Future studies are necessary to suggest alternatives to increase the accuracy of the QSM-derived metrics using UAV-LiDAR data. Furthermore, we suggest the assessment of other metrics, such as the crown length and crown ratio, which can be used as auxiliary variables in allometric equations and improve accuracy.

Author Contributions: Conceptualization, A.P.D.C., E.N.B.; methodology, A.P.D.C., F.E.R., B.N.d.V., D.R.A.d.A., C.R.S. and C.A.S.; software, M.M. and E.B.N.; formal analysis, A.P.D.C., F.E.R. and C.A.S.; investigation, A.P.D.C., D.R.A.d.A. and C.R.S.; resources, A.P.D.C., F.E.R., E.N.B. and A.d.M.; data curation, C.R.S., M.M., E.B.N. and A.M.A.Z.; writing—original draft preparation, A.P.D.C., F.E.R., B.N.d.V. and J.W.T., writing—review and editing, C.K., R.V.L., C.H.d.A., H.F.P.V., K.d.S.R., M.A.K., M.N.I.S. and E.N.B.; visualization, A.P.D.C., F.E.R. and B.N.d.V.; supervision, E.N.B. and A.d.M.; funding acquisition A.P.D.C., C.R.S., C.K. and E.N.B.; project administration, A.P.D.C. and E.N.B. All authors have read and agreed to the published version of the manuscript.

Institutional Review Board Statement: Not applicable for studies not involving humans or animals.

Informed Consent Statement: Not applicable.

Data Availability Statement: All datasets are available from the corresponding author.

Conflicts of Interest: The authors declare no conflict of interest.

References

1.　Barua, S.K.; Lehtonne, P.; Pahkasalo, T. Plantation vision: Potentials, challenges and policy options for global industrial forest plantation development. *Int. For. Rev.* **2014**, *16*, 117–127. [CrossRef]

2.　Schmidt, L.N.; Sanquetta, M.N.I.; McTague, J.P.; da Silva, G.F.; Fraga Filho, C.V.; Sanquetta, C.R.; Scolforo, J.R.S. On the use of Weibull distribution in modeling and describing diameter distributions of clonal eucalypt stands. *Can. J. For. Res.* **2020**, *50*, 1050–1063. [CrossRef]

3.　Shifley, S.R.; He, H.S.; Lischke, H.; Wang, W.J.; Jin, W.; Gustafson, E.J.; Thompson, J.R.; Thompson, F.R., III; Dijak, W.D.; Yang, J. The past and future of modeling forest dynamics: From growth and yield curves to forest landscape models. *Landsc. Ecol.* **2017**, *32*, 1307–1325. [CrossRef]

4.　Burkhart, H.E.; Tomé, M. *Modeling Forest Trees and Stands*, 1st ed.; Springer: Dordrecht, The Netherlands, 2012.

5.　Sanquetta, C.R.; Dalla Corte, A.P.; Pelissari, A.L.; Tomé, M.; Maas, G.C.B.; Sanquetta, M.N.I. Dynamics of carbon and CO2 removals by Brazilian forest plantations during 1990–2016. *Carbon Balance Manag.* **2018**, *13*, 20. [CrossRef] [PubMed]

6.　Indústria Brasileira de árvores (Ibá). Annual Report 2020. Available online: https://iba.org/datafiles/publicacoes/relatorios/relatorio-iba-2020.pdf (accessed on 15 September 2020).

7.　Heurich, M.; Thomas, F. Estimation of forestry stand parameters using laser scanning data in temperate, structurally rich natural European beech (Fagus sylvatica) and Norway spruce (Picea abies) forests. *Forestry* **2008**, *81*, 645–661. [CrossRef]

8.　Hyyppä, J.; Hyyppä, H.; Litkey, P.; Yu, W.; Haggrén, H.; Rönnholm, P.; Pyysalo, U.; Pitkänen, J.; Maltamo, M. Algorithms and methods of airborne laser scanning for forest measurements. *IEEE Trans. Geosci. Remote Sens.* **2001**, *39*, 969–975.

9. Vanclay, J.K. *Modeling Forest Growth and Yield: Applications to Mixed Tropical Forests*, 1st ed.; CAB International: Wallingford, UK, 1994.

10. Yu, X.; Hyyppä, J.; Vastaranta, M.; Holopainen, H.; Viitala, R. Predicting individual tree attributes from airborne laser point clouds based on the random forest technique. *ISPRS J. Photogramm. Remote Sens.* **2011**, *66*, 28–37. 08.003. [CrossRef]

11. Carnus, J.M.; Parrotta, J.; Brockerhoff, E.; Arbez, M.; Jactel, H.; Kremer, A.; Lamb, D.; O'Hara, K.; Walters, B. Planted forests and biodiversity. *J. For.* **2006**, *104*, 65–77. [CrossRef]

12. Spriggs, R.A.; Coomes, D.A.; Jones, T.A.; Caspersen, J.P.; Vanderwel, M.C. An alternative approach to using LiDAR remote sensing data to predict stem diameter distributions across a temperate forest landscape. *Remote Sens.* **2017**, *9*, 944. [CrossRef]

13. Woods, M.; Pitt, D.; Penner, M.; Lim, K.; Nesbitt, D.; Etheridge, D.; Treitz, P. Operational implementation of a LiDAR inventory in Boreal Ontario. *For. Chron.* **2011**, *87*, 512–528. [CrossRef]

14. Ye, N.; van Leeuwen, L.; Nyktas, P. Analysing the potential of UAV point cloud as input in quantitative structure modelling for assessment of woody biomass of single trees. *Int. J. Appl. Earth Observ.* **2019**, *81*, 47–57. [CrossRef]

15. Raumonen, P.; Kaasalainen, M.; Åkerblom, M.; Kaasalainen, S.; Kaartinen, H.; Vastaranta, M.; Holopainen, M.; Disney, M.; Lewis, P. Fast automatic precision tree models from terrestrial laser scanner data. *Remote Sens.* **2013**, *5*, 491–520. [CrossRef]

16. Chave, J.; Réjou-Méchain, M.; Búrquez, A.; Chidumaio, E.; Colgan, M.S.; Delitti, W.B.; Duque, A.; Eid, T.; Fearnside, P.M.; Goodman, R.C.; et al. Improved allometric models to estimate the aboveground biomass of tropical trees. *Glob. Chang. Biol.* **2014**, *20*, 3177–3190. [CrossRef] [PubMed]

17. Jara, M.C.; Henry, M.; Réjou-Méchain, M.; Wayson, C.; Zapata-Cuartas, M.; Piotto, D.; Guier, F.A.; Lombis, H.C.; López, E.C.; Lara, R.C.; et al. Guidelines for documenting and reporting tree allometric equations. *Ann. For. Sci.* **2015**, *72*, 763–768. [CrossRef]

18. Romero Ramirez, F.J.; Navarro-Cerrillo, R.M.; Varo-Martínez, M.Á.; Quero, J.L.; Doerr, S.; Hernández-Clemente, R. Determination of forest fuels characteristics in mortality-affected Pinus forests using integrated hyperspectral and ALS data. *Int. J. Appl. Earth Observ.* **2018**, *68*, 157–167. [CrossRef]

19. Dassot, M.; Colin, A.; Santenoise, P.; Fournier, M.; Constant, T. Terrestrial laser scanning for measuring the solid wood volume, including branches, of adult standing trees in the forest environment. *Comput. Electron. Agric.* **2012**, *89*, 86–93. [CrossRef]

20. Goodman, R.C.; Phillips, O.L.; Baker, T.R. The importance of crown dimensions to improve tropical tree biomass estimates. *Ecol. Appl.* **2014**, *24*, 680–698. [CrossRef]

21. Manuri, S.; Brack, C.; Nugroho, N.P.; Hergoualc'h, K.; Novita, N.; Dotzauer, H.; Verchot, L.; Putra, C.A.S.; Widyasari, E. Tree biomass equations for tropical forest ecosystem in Indonesia. *For. Ecol. Manag.* **2014**, *334*, 241–253. .2014.08.031. [CrossRef]

22. Corona, P.; Cartisano, R.; Salvati, R.; Chirici, G.; Floris, A.; Di Martino, P.; Marchetti, M.; Scrinzi, G.; Clementel, F.; Travaglini, D.; et al. Airborne laser scanning to support forest resource management under alpine, temperate and Mediterranean environments in Italy. *Eur. J. Remote Sens.* **2012**, *45*, 27–37. [CrossRef]

23. Popescu, S.C.; Zhao, K. A volex-based lidar method for estimating crown base height for deciduous and pine trees. *Remote Sens. Environ.* **2008**, *112*, 767–781. [CrossRef]

24. Wulder, M.A.; White, J.C.; Nelson, R.F.; Naesset, E.; Ørka, H.O.; Coops, N.C.; Hilker, T.; Bater, C.W.; Gobakken, T. Lidar sampling for large-area forest characterization: A review. *Remote Sens. Environ.* **2012**, *121*, 196–209. [CrossRef]

25. Hentz, A.M.K.; Silva, C.A.; Dalla Corte, A.P.; Péllico Netto, S.; Strager, M.P.; Klauberg, C. Estimating forest uniformity in Eucalyptus spp. and Pinus taeda L. stands using field measurements and structure from motion point clouds generated from unmanned aerial vehicle (UAV) data collection. *For. Ecosyst.* **2018**, *27*, e005. [CrossRef]

26. Mohan, M.; Silva, C.A.; Klauberg, C.; Jat, P.; Catts, G.; Cardil, A.; Hudak, A.T.; Dia, M. Individual tree detection from unmanned aerial vehicle (UAV) derived canopy height model in an Open Canopy Mixed Conifer Forest. *Forests* **2017**, *8*, 340. [CrossRef]

27. Rex, F.E.; Dalla Corte, A.P.; Machado, S.A.; Silva, C.A.; Sanquetta, C.R. Estimating above-ground biomass of Araucaria angustifolia (Bertol.) Kuntze using LiDAR data. *Floresta Ambiente* **2019**, *26*, e20171107. [CrossRef]

28. Rex, F.E.; Silva, C.A.; Dalla Corte, A.P.; Klauberg, C.; Mohan, M.; Cardil, A.; da Silva, V.S.; de Almeida, D.R.; Garcia, M.; Broadbent, E.N.; et al. Comparison of statistical modelling approaches for estimating Tropical Forest aboveground biomass stock and reporting their changes in low-intensity logging areas using multi-temporal LiDAR data. *Remote Sens.* **2020**, *12*, 1498. [CrossRef]

29. Silva, C.A.; Valbuena, R.; Pinagé, E.R.; Mohan, M.; de Almeida, D.R.A.; Broadbent, E.N.; Jaafar, W.S.W.M.; Papa, D.A.; Cardil, A.; Klauberg, C. ForestGAPR: An R package for forest gap analysis from canopy height models. *Methods Ecol. Evol.* **2019**, *10*, 1347–1356. [CrossRef]

30. Wan Mohd Jaafar, W.S.; Woodhouse, I.H.; Silva, C.A.; Omar, H.; Maulud, K.N.A.; Hudak, A.T.; Klauberg, C.; Cardil, A.; Mohan, M. Improving individual tree crown delineation and attributes estimation of Tropical Forests using airborne LiDAR data. *Forests* **2018**, *9*, 759. [CrossRef]

31. Brede, B.; Calders, K.; Lau, A.; Raumonen, P.; Bartholomeus, H.M.; Herold, M.; Kooistra, L. Non-destructive tree volume estimation through quantitative structure modelling: Comparing UAV laser scanning with terrestrial LIDAR. *Remote Sens. Environ.* **2019**, *233*, 111355. [CrossRef]

32. Malhi, Y.; Jackson, T.; Patrick Bentley, L.; Lau, A.; Shenkin, A.; Herold, M.; Calders, K.; Bartholomeus, H.; Disney, M.I. New perspectives on the ecology of tree structure and tree communities through terrestrial laser scanning. *Interface Focus* **2018**, *8*, 20170052. [CrossRef]

33. Wilkes, P.; Lau, A.; Disney, M.; Calders, K.; Burt, A.; de Tanago, J.G.; Bartholomeus, H.; Brede, B.; Herold, M. Data acquisition considerations for Terrestrial Laser Scanning of forest plots. *Remote Sens. Environ.* **2017**, *196*, 140–153. [CrossRef]

34. Kaasalainen, S.; Krooks, A.; Liski, J.; Raumonen, P.; Kaartinen, H.; Kaasalainen, M.; Puttonen, E.; Anttila, K.; Mäkipää, R. Change detection of tree biomass with terrestrial laser scanning and quantitative structure modelling. *Remote Sens.* **2014**, *6*, 3906–3922. [CrossRef]

35. Hosoi, F.; Nakai, Y.; Omasa, K. 3-D voxel-based solid modeling of a broad-leaved tree for accurate volume estimation using portable scanning lidar. *ISPRS J. Photogramm. Remote Sens.* **2013**, *82*, 41–48. [CrossRef]

36. Lefsky, M.A.; McHale, M.R. Volume estimates of trees with complex architecture from terrestrial laser scanning. *J. Appl. Remote Sens.* **2008**, *2*, 023521. [CrossRef]

37. Calders, K.; Burt, A.; Newnham, G.; Disney, M.; Murphy, S.; Raumonen, P.; Herold, M.; Culvenor, D.; Armston, J.; Avitabile, V.; et al. Reducing uncertainties in above-ground biomass estimates using terrestrial laser scanning. *Proc. Silvilaser* **2015**, *6*, 197–199.

38. Côté, J.F.; Widlowski, J.L.; Fournier, R.A.; Verstraete, M.M. The structural and radiative consistency of three-dimensional tree reconstruction from terrestrial lidar. *Remote Sens. Environ.* **2009**, *113*, 1067–1081. [CrossRef]

39. Côté, J.; Fournier, R.A.; Egli, R. An architectural model of trees to estimate forest structural attributes using terrestrial LiDAR. *Environ. Model. Softw.* **2011**, *26*, 761–777. [CrossRef]

40. Hackenberg, J.; Morhart, C.; Sheppard, J.; Spiecker, H.; Disney, M.I. Highly accurate tree models derived from terrestrial laser scan data: A method description. *Forests* **2014**, *5*, 1069–1105. [CrossRef]

41. Mayamanikandan, T.; Reddy, R.S.; Jha, C.S. Non-destructive tree volume estimation using terrestrial LiDAR data in teak dominated central Indian forests. In Proceedings of the IEEE Recent Advances in Geoscience and Remote Sensing: Technologies, Standards and Applications (TENGARSS), Kochi, India, 17–20 October 2019; pp. 100–103.

42. Terryn, L.; Calders, K.; Disney, M.; Origo, N.; Malhi, Y.; Newnham, G.; Raumonen, P.; Åkerblom, H.V.; Verbeeck, H. Tree species classification using structural features derived from terrestrial laser scanning. *ISPRS J. Photogramm. Remote Sens.* **2020**, *168*, 170–181. [CrossRef]

43. Disney, M.I.; Boni Vicari, M.; Burt, A.; Calders, K.; Lewis, S.L.; Raumonen, P.; Wilkes, P. Weighing trees with lasers: Advances, challenges and opportunities. *Interface Focus* **2018**, *8*, 20170048. [CrossRef]

44. Du, S.; Lindenbergh, R.; Ledoux, H.; Stoter, J.; Nan, L. AdTree: Accurate, detailed, and automatic modelling of laser-scanned trees. *Remote Sens.* **2019**, *11*, 2074. [CrossRef]

45. Kunz, M.; Hess, C.; Raumonen, P.; Bienert, A.; Hackenberg, J.; Maas, H.; Härdtle, W.; Fichtner, A.; Oheimb, G.V. Comparison of wood volume estimates of young trees from terrestrial laser scan data. *iForest* **2017**, *10*, 458–541. [CrossRef]

46. Markku, Å.; Raumonen, P.; Kaasalainen, M.; Casella, E. Analysis of geometric primitives in quantitative structure models of tree stems. *Remote Sens.* **2015**, *7*, 4581–4603. [CrossRef]

47. Silva, C.A.; Klauberg, C.; Hudak, A.T.; Vierling, L.A.; Jaafar, W.S.W.M.; Mohan, M.; Garcia, M.; Ferraz, A.; Cardil, A.; Saatchi, S. Predicting stem total and assortment volumes in an industrial Pinus taeda L. forest plantation using airborne laser scanning data and random forest. *Forests* **2017**, *8*, 254. [CrossRef]

48. Zhang, W.; Wan, P.; Wang, T.; Cai, S.; Chen, Y.; Jin, X.; Yan, G. A novel approach for the detection of standing tree stems from plot-level terrestrial laser scanning data. *Remote Sens.* **2019**, *11*, 211. [CrossRef]

49. Dalla Corte, A.P.; Rex, F.E.; de Almeida, D.R.A.; Sanquetta, C.R.; Silva, C.A.; Moura, M.M.; Wilkinson, B.; Zambrano, A.M.A.; da Cunha Neto, E.M.; Veras, H.F.P.; et al. Measuring individual tree diameter and height using GatorEye high-density UAV-Lidar in an integrated crop-livestock-forest system. *Remote Sens.* **2020**, *12*, 863. [CrossRef]

50. Dalla Corte, A.P.; Souza, D.V.; Rex, F.E.; Sanquetta, C.R.; Mohan, M.; Silva, C.A.; Zambrano, A.A.; Prata, G.; de Almeida, D.R.A.; Trautenmüller, J.W.; et al. Forest inventory with high-density UAV-Lidar: Machine learning approaches for predicting individual tree attributes. *Comput. Electron. Agric.* **2020**, *179*, 105815. [CrossRef]

51. Instituto Brasileiro de Geografia e Estatística (IBGE)— Embrapa. *Mapa de Solos do Brasil (Scale 1:5,000,000)*; Embrapa Solos: Rio de Janeiro, Brazil, 2001.

52. Soil Survey Staff. *Key to Soil Taxonomy*, 11th ed.; U.S. Department of Agriculture, Natural Resources Conservation Service: Washington, DC, USA, 2010.

53. Alvares, C.A.; Stape, J.L.; Sentelhas, P.C.; Gonçalves, J.L.M.; Sparovek, G. Köppen's climate classification map for Brazil. *Meteorol. Z.* **2013**, *22*, 711–728. [CrossRef]

54. Wilkinson, B.; Lassiter, H.A.; Abd-Elrahman, A.; Carthy, R.R.; Ifju, P.; Broadbent, E.N.; Grimes, N. Geometric targets for UAS lidar. *Remote Sens.* **2019**, *11*, 3019. [CrossRef]

55. Broadbent, E.N.; Zambrano, A.M.A.; Omans, G.; Adler, B.; Alonso, P.; Naylor, D.; Chenevert, G.; Murtha, T.; Almeida, D.R.A.; Dalla Corte, A.P.; et al. In prep. The GatorEye Unmanned Flying Laboratory: Sensor Fusion for 4D Ecological Analysis through Custom Hardware and Algorithm Integration. In prep. 2020. Available online: http://www.gatoreye.org (accessed on 10 September 2020).

56. Isenburg, M. "LAStools—Efficient LiDAR Processing Software" (Version 1.8, Licensed). Available online: http://rapidlasso.com/LAStools (accessed on 11 November 2019).

57. R Core Team. R: A Language and Environment for Statistical Computing. R Foundation for Statistical Computing. 2018. Available online: https://www.r-project.org/ (accessed on 10 September 2021).

58. Dalponte, M.; Coomes, D.A. Tree-centric mapping of forest carbon density from airborne laser scanning and hyperspectral data. *Methods. Ecol. Evol.* **2016**, *7*, 1236–1245. [CrossRef]

59. Roussel, J.R.; Auty, D.; Coops, N.C.; Tompalski, P.; Goodbody, T.R.; Meador, A.S.; Bourdon, J.F.; de Boissieu, F.; Achim, A. lidR: An R package for analysis of Airborne Laser Scanning (ALS) data. *Remote Sens. Environ.* **2020**, *251*, 112061. [CrossRef]

60. Åkerblom, M.; Raumonen, P.; Casella, E.; Disney, M.I.; Danson, F.M.; Gaulton, R.; Schofield, L.A.; Kaasalainen, M. Non-intersecting leaf insertion algorithm for tree structure models. *Interface Focus* **2018**, *8*, 20170045. [CrossRef]

61. Raumonen, P.; Casella, E.; Calders, K.; Murphy, S.; Åkerblom, M.; Kaasalainen, M. Massive-scale tree modelling from TLS data. ISPRS Ann. Photogramm. *Remote Sens. Spat. Inf. Sci.* **2015**, *2*, 189–196. [CrossRef]

62. Spurr, S.H. *Forest Inventory*, 1st ed.; Ronald Press Co.: New York, NY, USA, 1952.

63. Wan Mohd Jaafar, W.S.; Abdul Maulud, K.N.; Muhmad Kamarulzaman, A.M.; Raihan, A.; Md Sah, S.; Ahmad, A.; Saad, S.N.M.; Mohd Azmi, A.T.; Jusoh Syukri, N.K.A.; Razzaq Khan, W. The influence of deforestation on land surface temperature — A case study of Perak and Kedah, Malaysia. *Forests* **2020**, *11*, 670. [CrossRef]

64. White, J.C.; Coops, N.C.; Wulder, M.A.; Vastaranta, M.; Hilker, T.; Tompalski, P. Remote sensing technologies for enhancing forest inventories: A review. *Can. J. Remote. Sens.* **2016**, *42*, 619–641. [CrossRef]

65. Kangas, A.; Astrup, R.; Breidenbach, J.; Fridman, J.; Gobakken, T.; Korhonen, K.T.; Maltamo, M.; Nilsson, M.; Nord-Larsen, T.; Næsset, E.; et al. Remote sensing and forest inventories in Nordic countries—roadmap for the future. *Scand. J. For. Res.* **2018**, *33*, 397–412. [CrossRef]

66. Wu, X.; Shen, X.; Cao, L.; Wang, G.; Cao, F. Assessment of individual tree detection and canopy cover estimation using unmanned aerial vehicle based light detection and ranging (UAV-Lidar) data in planted forests. *Remote Sens.* **2019**, *11*, 908. [CrossRef]

67. Almeida, D.R.A.; Stark, S.C.; Chazdon, R.; Nelson, B.W.; Cesar, R.G.; Meli, P.; Gorgens, E.B.; Duarte, M.M.; Valbuena, R.; Moreno, V.S.; et al. The effectiveness of lidar remote sensing for monitoring forest cover attributes and landscape restoration. *For. Ecol. Manag.* **2019**, *438*, 34–43. [CrossRef]

68. Melo, A.M.; Reis, C.R.; Martins, B.F.; Penido, T.M.A.; Rodriguez, L.C.E.; Gorgens, E.B. Monitoring the understory in eucalyptus plantations using airborne laser scanning. *Sci. Agric.* **2020**, *78*, e20190134. [CrossRef]

69. Brodu, N.; Lague, D. 3D terrestrial lidar data classification of complex natural scenes using a multi-scale dimensionality criterion: Applications in geomorphology. *ISPRS J. Photogramm. Remote Sens.* **2012**, *68*, 121–134. [CrossRef]

70. Kim, E.; Medioni, G. Urban scene understanding from aerial and ground LIDAR data. *Mach. Vis. Appl.* **2011**, *22*, 691–703. [CrossRef]

71. Kankare, V.; Holopainen, M.; Vastaranta, M.; Puttonen, E.; Yu, X.; Hyyppä, J.; Maaja, M.; Hyyppä, H.; Alho, P. Individual tree biomass estimation using terrestrial laser scanning. *ISPRS J. Photogramm. Remote Sens.* **2013**, *75*, 64–75. [CrossRef]

72. Pitkänen, T.P.; Raumonen, P.; Kangas, A. Measuring stem diameters with TLS in boreal forests by complementary fitting procedure. *ISPRS J. Photogramm. Remote Sens.* **2019**, *147*, 294–306. [CrossRef]

73. Wan Mohd Jaafar, W.S.; Woodhouse, I.H.; Silva, C.A.; Omar, H.; Hudak, A.T. Modelling individual tree aboveground biomass using discrete return lidar in lowland dipterocarp forest of Malaysia. *J. Trop. For. Sci.* **2017**, *29*, 465–484. [CrossRef]

74. Wang, L.; Muralikrishnan, B.; Rachakonda, P.; Sawyer, D. Determining geometric error model parameters of a terrestrial laser scanner through Two-face, Length-consistency, and Network methods. *Meas. Sci. Technol.* **2017**, *28*, 065016. [CrossRef]

75. Morales, G.; Kemper, G.; Sevillano, G.; Arteaga, D.; Ortega, I.; Telles, J. Automatic segmentation of Mauritia flexuosa in unmanned aerial vehicle (UAV) imagery using deep learning. *Forests* **2018**, *9*, 736. [CrossRef]

76. Cerqueira, C.L.; Arce, J.E.; Vendruscolo, D.G.S.; Dolácio, C.J.F.; Costa Filho, S.V.S.; Tonini, H. Tape modeling of eucalyptus stem in crop-livestock-forestry integration system. *Floresta* **2019**, *49*, 493–502. [CrossRef]

77. Arias-Rodil, M.; Diéguez-Aranda, U.; Burkhart, H.E. Effects of measurement error in total tree height and upper-stem diameter on stem volume prediction. *For. Sci.* **2017**, *63*, 250–260. [CrossRef]

78. Sanquetta, C.R.; Behling, A.; Dalla Corte, A.P.; Péllico Netto, S.; Schikowski, A.B.; do Amaral, M.K. Simultaneous estimation as alternative to independent modeling of tree biomass. *Ann. For. Sci.* **2015**, *72*, 1099–1112. [CrossRef]

79. Krooks, A.; Kaasalainen, S.; Kankare, V.; Joensuu, M.; Raumonen, P.; Kaasalainen, M. Predicting tree structure from tree height using terrestrial laser scanning and quantitative structure models. *Silva Fennica* **2014**, *48*, 1125. [CrossRef]

80. Smith, A.L.; Astrup, R.; Raumonen, P.; Liski, J.; Krooks, A.; Kaasalainen, S.; Åkerblom, M.; Kaasalainen, M. Tree root system characterization and volume estimation by Terrestrial Laser Scanning and Quantitative Structure Modelling. *Forests* **2014**, *5*, 3274–3294. [CrossRef]